EPJ Web of Conferences **72**, 00014 (2014)
DOI: 10.1051/epjconf/20147200014


# Research with real photons at the MAMI 1.6 GeV electron accelerator

I J Douglas MacGregor[1,a], for the A2-CB Collaboration

[1]SUPA School of Physics and Astronomy, University of Glasgow, Glasgow G12 8QQ, UK

**Abstract.** The A2-CB Collaboration at Mainz is studying the structure of hadrons by meson photoproduction using unpolarised, linearly polarised and circularly polarised photons with energies up to 1.6 GeV. Photons are energy-tagged using the Glasgow-Mainz tagged photon spectrometer and a new high-energy end-point tagger which allows η' reactions to be studied. Reaction products are detected in a ~4π detector consisting of the Crystal Ball detector and TAPS forward wall. Transverse or longitudinally polarised proton targets are available and new techniques have been developed to measure the polarisation of recoiling protons. These facilities have allowed an extensive programme of double-polarisation meson-photoproduction experiments to be carried out to search for so-called "missing baryon resonances" on proton and deuteron targets. Searches have also been carried out to investigate narrow resonances in the η-photoproduction channel at invariant masses around 1680 MeV. Coherent $\pi^0$ production measurements have been used to estimate the neutron skin thickness in $^{208}$Pb. This paper presents selected highlights from the A2-CB collaboration research programme at MAMI.

## 1 Introduction

The 1.6 GeV Mainz electron microtron MAMI [1, 2] is a world-class facility for nuclear and hadron physics studies. It provides a low emittance 100% duty factor electron beam which is used for experiments with real and virtual photons. This paper describes a range of meson production experiments carried out using real photons, including studies of the spectrum of baryon resonances, the existence of narrow nucleon resonances, production of strange mesons and measurements of the neutron skin thicknesses in heavy nuclei.

## 2 The real photon facility at MAMI

This section describes the MAMI electron beam facility, the Glasgow-Mainz photon tagging spectrometer, the Crystal Ball and TAPS detector systems and the apparatus and techniques used for polarising proton targets and measuring proton recoil polarisation.

### 2.1 The 1.6 GeV MAMI electron microtron facility

The MAMI electron accelerator [1, 2] consists of three cascaded racetrack microtrons (RTM 1-3) and one harmonic double-sided microtron (HDSM) (see figure 1). A 3.5 MeV linac injector feeds into RTM1, an 18 turn racetrack microtron, which raises the beam energy to 15 MeV. RTM2 has 51 recirculations, raising the energy to 180 MeV. RTM 3, with 90 turns, produces an output of 855 MeV. The final stage is a 43 turn harmonic double-sided microtron which raises the electron energy to a maximum of 1.608 GeV. Lower energies can be extracted in ~15 MeV steps by using a smaller number of recirculations. The final beam energy is very well determined by the constraints imposed by recirculation and has a spread of only ~110 keV.

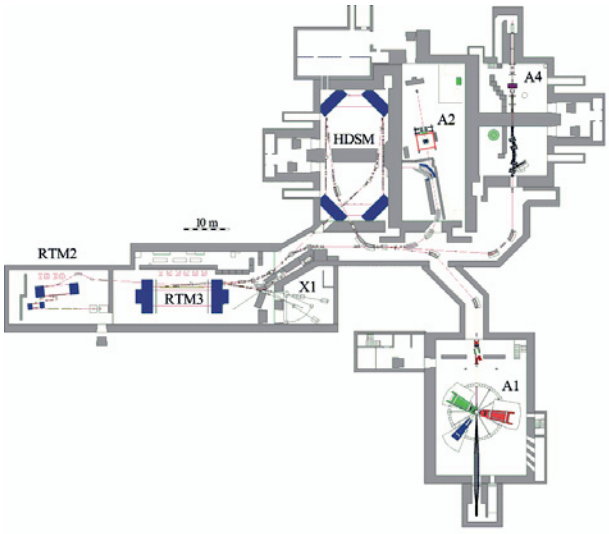


**Figure 1.** Schematic diagram of the MAMI 1.6 GeV electron microtron facility.

[a] Corresponding author: douglas.macgregor@glasgow.ac.uk

The 1.6 GeV beam is transported to one of four detector halls for experiments with real photons (A2), virtual photons (A1), parity-violating electron scattering (A4) or brilliant x-ray radiation sources (X1).

### 2.2 The Glasgow-Mainz Photon Tagger

Bremsstrahlung photons are produced by directing the electron beam onto a thin radiator. The resulting photon beam is collimated onto a target placed in the centre of the Crystal Ball detector (see section 2.3). The recoil bremsstrahlung electrons are energy-tagged in the Glasgow-Mainz Tagged Photon Spectrometer [3-5], allowing the energies of the photons to be determined on an event-by-event basis. The scattered electrons are momentum analysed in a large dipole magnet and are detected in a focal plane detector (FPD) consisting of 353 overlapping plastic scintillators. The energy width of each channel ranges from ~2 MeV at the highest tagged photon energies to ~4 MeV at lower energies.

The Glasgow-Mainz photon tagger can measure the energies of photons up to $E_\gamma$~1.495 GeV. To access higher energies a separate End-Point Tagger (EPT) has recently been installed. This consists of a ~1.2 T dipole magnet with its own focal plane detector array. It is capable of tagging photons in the energy range $E_\gamma$= 1.458–1.598 GeV. The threshold for η' decay is $E_\gamma$=1.447 and one of the main aims of the EPT is to carry out detailed studies of η' decay modes [6].

**Figure 2.** The Glasgow-Mainz Tagger Microcope detector.

For high-resolution studies a "microscope" detector [7], consisting of 96 2x3 $mm^2$ cross-section scintillating fibres, coupled to six multi-anode PMTs, has been constructed (see figure 2). The microscope is located immediately in front of the tagger FPD. It spans a photon energy range of ~100 MeV with a photon energy resolution ~5 times better than the standard focal plane detector.

Linearly polarised photons are produced using coherent bremsstrahlung from a thin (~100 μm) diamond crystal radiator [8, 9]. The diamond is oriented using a goniometer with an initial alignment carried out using the Stonehenge technique [10]. Photon polarisation typically occurs in a peak of width ~100 MeV. The peak energy and the maximum polarisation which can be achieved depend on the electron beam energy and the orientation of the diamond crystal. Figure 3 shows the calculated photon polarisation achievable in a number separate diamond alignments. Tight collimation of the photon beam is used to further enhance the average photon polarisation.

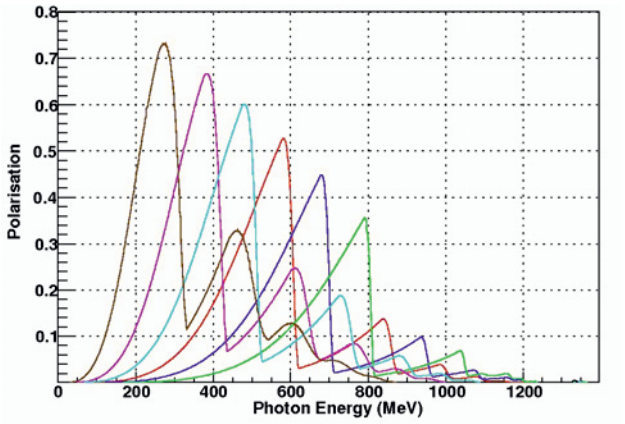


**Figure 3.** Degree of linear photon polarisation achievable at MAMI in a number of diamond orientations.

In addition, circularly polarised photons can be produced by helicity transfer from a longitudinally polarised electron beam. At MAMI circular polarisation up to ~85% is possible.

### 2.3 The Crystal Ball and TAPS

Reaction products are detected in the Crystal Ball (CB) [11] and TAPS [12, 13] detector arrays. Neutral pions and η-mesons are principally detected via their photon decay modes (e.g. $\pi^0 \rightarrow 2\gamma$). In addition to measuring photon momenta, the detector arrays are also capable of detecting protons and charged mesons. Proton detection is important in determining the recoil polarisation in meson photoproduction experiments.

The CB [11] is a highly segmented total energy calorimeter consisting of 672 NaI crystals with a thickness of ~15.7 $X_0$ (radiation lengths). It covers ~94% of 4π sr, with entrance and exit holes at polar angles $\theta>160^o$ and $\theta<20^o$ with respect to the photon beam axis. The energy of each particle detected in the CB is reconstructed from the total energy deposited in a cluster of adjacent crystals.

Charged particles are identified using their differential energy loss measured in a Particle Identification Detector (PID) [14], mounted inside the Crystal Ball, together with the energy deposited in the CB. The PID also provides trigger timing information for events with one or more charged particles in the final state. It consists of 24 scintillators (31 cm long, 13mm wide and 2mm thick) arranged to form a 10 cm diameter barrel. Charged particle tracking is provided by two MWPC wire chambers mounted between the CB and the PID.

Forward-going particles ($\theta<20^o$) are detected in the TAPS detector array [12, 13], consisting of 384 $BaF_2$ crystals (~12 $X_0$), configured as a forward wall. The innermost six $BaF_2$ crystals have been replaced by 24 smaller $PbWO_4$ (~ 22 $X_0$) crystals to handle higher event counting rates. For the identification of charged particles, 5mm thick plastic veto-scintillators [15] were mounted in front of the $BaF_2$ crystals.

### 2.4 Frozen spin target and recoil polarimetry

Polarised targets are provided using a frozen spin butanol ($C_4H_9OH$) system [16] which can polarise protons either longitudinally or transversely to the photon beam. Polarised neutrons are provided using deuterated butanol.

The 2cm long target cell is maintained at a temperature of 25 mK using a $^3$He/$^4$He dilution refrigerator (see figure 4). The whole apparatus fits inside the PID detector at the centre of the CB. The target is polarised externally and inserted into the CB. Internal holding coils, with a magnetic field of ~0.45 T, maintain the polarisation which is typically in excess of 90%. The holding coils are as thin as possible to allow particles to pass through to the detectors. The target has proved to be stable and reliable with a relaxation time in excess of 1000 hours.

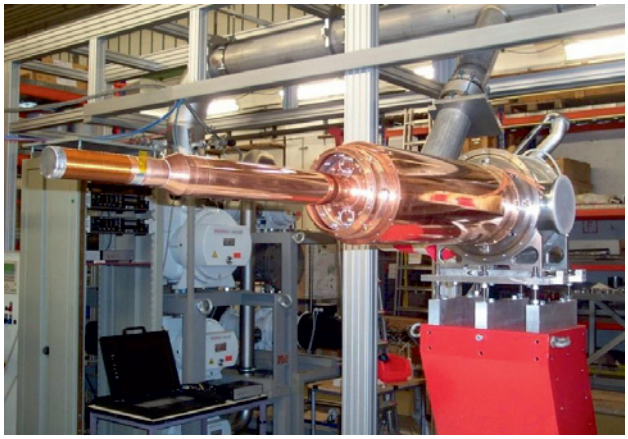

**Figure 4.** The Mainz dilution refrigerator and frozen spin target.

Measurements of the polarisation of the recoil proton in $p(\gamma,\pi^0)p$ experiments are made using a novel technique [17]. A 2.25 cm thick graphite cylinder with a 7.25 cm endcap is located around the target to act as a polarimeter. The recoil proton momentum is calculated from the photon energy and the measured pion energy using two-body kinematics. The measured proton angle then allows the scattering in the polarimeter to be deduced.

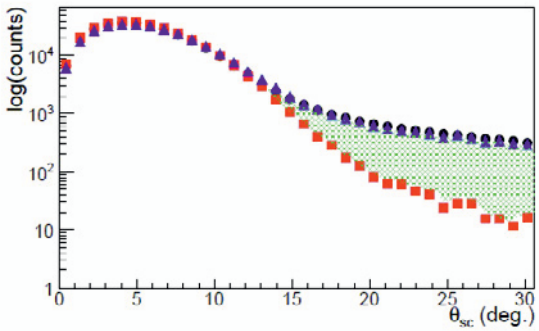


**Figure 5.** Comparison of $\theta_{sc}$ for data (blue circles) and simulation (blue triangles). The simulation with no hadronic interaction is shown by red squares. Nuclear scattered events lie in the green shaded region.

The azimuthal scattering angle depends on the recoil polarisation P and the analysing power of the polarimeter. Figure 5 shows that appreciable nuclear scattering only occurs for polar scattering angles above ~15°. However, data in this region, together with a knowledge of the proton-$^{12}$C analysing power can be used to extract the polarisation P of the recoil proton.

## 3 Selected meson photoproduction experiments

This section describes four recent experiments carried out at the 1.6 GeV MAMI electron beam facility which each look at different aspects of meson photoproduction.

### 3.1 Double-polarised pion photoproduction

Fewer nucleon resonances have been unambiguously observed than are predicted by QCD models [18, 19]. Most of the previous evidence for these resonances comes from pion-nucleon scattering. To investigate whether these resonances are really "missing" or are simply difficult to observe due to small cross sections amongst the overlapping tails of a few dominant resonances, a major pseudoscalar meson photoproduction programme has been initiated at many labs including Mainz, Bonn and Jefferson Laboratory.

**Table 1.** Observables in pseudoscalar meson photoproduction. Those listed in blue have already been measured for the $p(\gamma,\pi^0)$ reaction at MAMI. Those in green are currently being measured.

| | Observable | Polarisation | | |
|---|---|---|---|---|
| | | Beam | Target | Recoil |
| Unpolarised | $\sigma_0$ | | | |
| Single Polarisation | $\Sigma$ | Linear | | |
| | T | | y' | |
| | P | | | y' |
| Double Polarisation Beam-Target | E | Circ. | Long. | |
| | F | Circ. | Trans. | |
| | G | Linear | Long. | |
| | H | Linear | Trans. | |
| Double Polarisation Beam-Recoil | $C_x$ | Circ. | | x' |
| | $C_z$ | Circ. | | z' |
| | $O_x$ | Linear | | x' |
| | $O_z$ | Linear | | z' |
| Double Polarisation Target-Recoil | $T_x$ | | Trans. | x' |
| | $T_z$ | | Trans. | z' |
| | $L_x$ | | Long. | x' |
| | $L_z$ | | Long. | z' |

The mechanism for pseudoscalar meson photoproduction is determined by four complex transversity amplitudes [20]. Cross section measurements only provide access to the sum of the squared magnitudes of these amplitudes. For a full understanding it is necessary to measure a range of single- and double-polarisation observables. These require studies with

linearly and circularly polarised photons, measurements with transversely and longitudinally polarised targets and measurements of nucleon recoil polarisation.

Table 1 lists the possible single and double polarisation observables which can be measured and indicates which of these are being studied for the $p(\gamma,\pi^0)$ reaction at MAMI. For a complete determination of the transversity amplitudes it is necessary to measure at least eight of these observables, including at least one from each section of the table [21].

To give a flavour of the quality of the data obtained at MAMI, Figure 6 shows preliminary data for T and F, presented as a function of the centre-of-mass pion polar angle. The data are compared with calculations using the MAID, SAID and Bonn-Gatchina meson photo-production models. While the models describe the main trends in the data it is clear that they do not agree in detail and that the preliminary data provide new information to distinguish between them, particularly at higher photon energies.

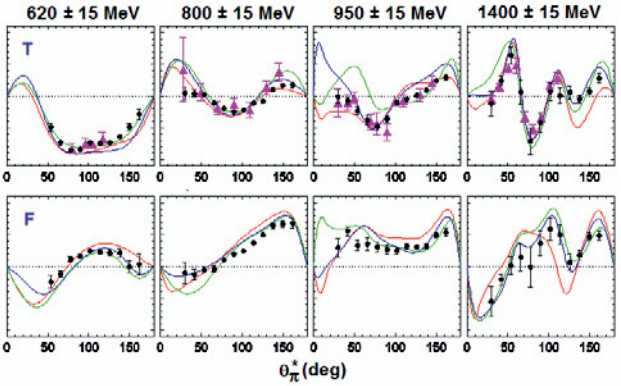


**Figure 6.** Preliminary angular distributions for T and F presented as function of centre-of-mass pion polar angle, for selected photon energy bins. The black data are preliminary measurements from MAMI. The magenta triangles are world data before 2000. The data are compared to three models: MAID 2007 (green line); SAID CM12 (blue line) and BG2011-02 (red line).

### 3.2 η photoproduction

Evidence of a narrow $N^*$ nucleon resonance structure around 1.685 GeV has been found in η photoproduction from neutron targets in recent years. The GRAAL collaboration observed a narrow structure in the quasi-free neutron cross section and in the ηn invariant mass spectrum around this energy [22]. The CBELSA/TAPS collaboration also reported narrow structure in the neutron cross section at W~1.68 GeV [23].

Neither experiment found any evidence for a narrow structure in the proton channel. This may be due to the predicted weaker photo-coupling between the $N^*(1685)$ and the proton, as compared to the neutron case. The quark model that predicts the $N^*(1685)$ states that excitation of the resonance on the proton would require explicit SU(3) symmetry breaking, with a strength that depends linearly on the strange current quark mass [24].

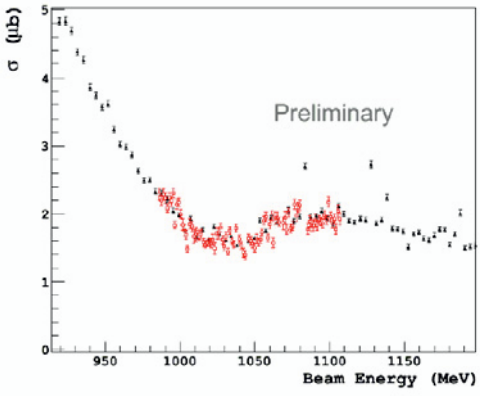


**Figure 7.** Preliminary cross sections for η photoproduction as a function of photon energy. The black data points were taken with the tagger FPD. The red data points were obtained using the high-resolution tagger microscope.

In order to investigate the proton channel with high resolution an experiment [25, 26] was carried out using the tagger microscope [7] and a liquid hydrogen target. η-mesons were selected using a 3σ cut on the invariant masses of all 2γ-decay events. The missing mass of the system was then reconstructed, showing a clear proton peak.

Figure 7 shows the preliminary cross sections obtained from this analysis, as a function of photon energy. Neither the data obtained from the tagger FPD nor from the tagger microscope shows any sign of a narrow resonance at $E_\gamma$=1.045 GeV, the photon energy corresponding to W= 1.685 GeV.

### 3.3 Photoproduction of $K^+$ mesons

The measurement of strange meson photo-production is complicated by large backgrounds from non-strange particles. However, a unique identification of charged kaons [27] can be made by their muonic decay mode: $K^+ \rightarrow \mu^+ \nu_\mu$. This technique makes use of the energy and timing of the signals in the segmented CB detector array.

As depicted in figure 8, each CB event is split into two sub-clusters. The "incident-cluster" (IC, blue) consists of those crystals in prompt coincidence (±10ns) with the photon tagger and which have a summed energy deposit greater than 25 MeV. Crystals with timings greater than 10ns are assumed to be part of the "decay cluster" (DC, red) corresponding to detection of the decay muon. A minimum summed DC energy of 75 MeV with signals in four or more crystals is required. The numbers of such DC events exhibit an exponential decay with a half-life corresponding to the muonic decay of charged kaons.

This technique was used to study both the $p(\gamma,K^+)\Lambda$ and $p(\gamma,K^+)\Sigma^0$ reactions. These two reactions were separated by looking for a coincidence with the γ-ray from the $\Lambda \rightarrow \Sigma^0\gamma$ decay. A GEANT4 Monte Carlo simulation was carried out to determine the γ–detection efficiency.

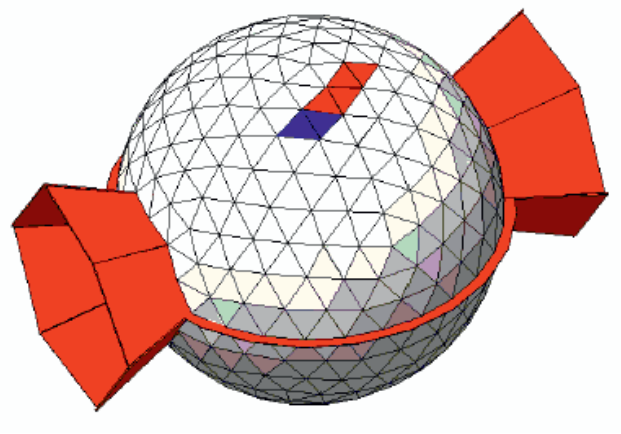

**Figure 8.** Identification of charged kaons in the CB. The blue crystals denote the incident cluster (IC) and the red crystals (DC) the cluster of crystals with signals from a subsequent muonic decay.

Figures 9 and 10 show samples of the differential cross sections obtained for the $p(\gamma,K^+)\Sigma^0$ and $p(\gamma,K^+)\Lambda$ reactions, respectively, compared to the previous world data [28-31].

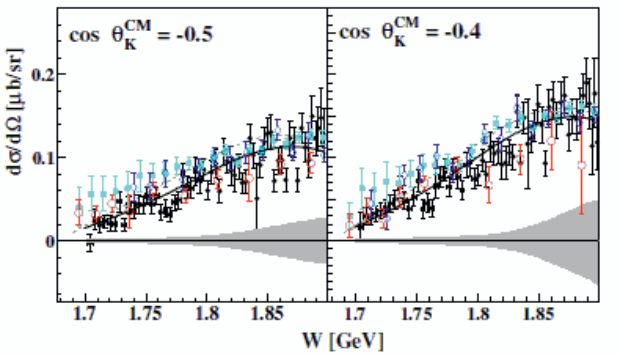


**Figure 9.** Differential cross sections for $p(\gamma,K^+)\Sigma^0$ as a function of W for selected $K^+$ centre-of-mass angular bins. MAMI data (black), with systematic uncertainties indicated by the grey shaded band, are compared to previous data from SAPHIR [28] (red), CLAS [29] (blue) and CLAS [30] (cyan). The solid black line is the BnGa 2011-02 prediction, fitted to include the new data.

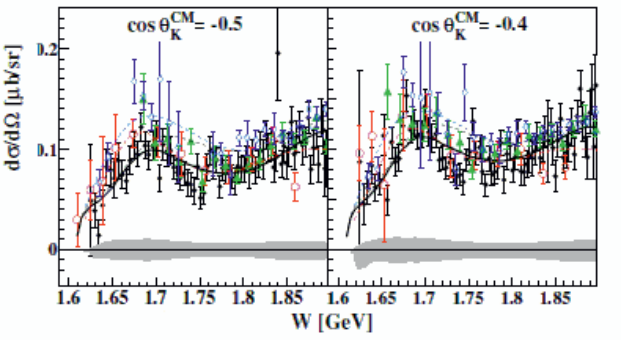


**Figure 10.** Differential cross sections for $p(\gamma,K^+)\Lambda$ as a function of W for selected $K^+$ centre-of-mass angular bins. Data are as described in figure 9 with additional CLAS data [31] (green).

The new data are in good agreement with previous work [28-31], but have better centre-of-mass energy resolution and statistical accuracy. They are able to provide valuable new constraints on models of strange meson photoproduction.

### 3.4 Coherent $\pi^0$ production experiments

The charge radii of nuclei are very well determined by elastic electron scattering. However, heavy nuclei have many more neutrons than protons and it is essential to determine their neutron distributions in order to fully understand the basic size and structure of nuclei. Recently a new technique, coherent $\pi^0$ production, has been used to measure the neutron radius and the neutron skin thickness in $^{208}$Pb [32].

Naïvely one expects neutrons and protons to have similar densities and hence the neutron distribution will extend further than the proton distribution, creating a neutron skin. In this surface region there will be significantly more neutrons than protons, changing the isospin balance. It is therefore not surprising that nuclear theories [33] show a strong correlation between neutron skin and the nuclear symmetry energy.

One way of describing the neutron skin is in term of $\Delta r_{pn}$ the difference in rms radii for the neutron and proton distributions. Recent analyses of proton [34] and pion [35] scattering data give $\Delta r_{pn}$ = 0.211 ± 0.06 fm and 0.16 ± 0.07 fm respectively. Measurements of the annihilation of antiprotons on the surface of nuclei [36, 37] give values of 0.18 ± 0.04 (exp) ± 0.05 (theory) fm. Analyses of isospin diffusion in heavy-ion collisions give 0.22±0.04 fm [38]. A recent prediction based on measurements of the pygmy dipole resonance in lighter nuclei gives 0.194±0.024 fm in $^{208}$Pb [39-41]. However the interpretation of this resonance and the model dependence of the result is still a matter of discussion [42]. Parity violating electron scattering on nuclei (PREX), utilising the preferential coupling of the exchanged weak boson to neutrons gave a first measurement, at a single momentum transfer, of 0.33±0.17 fm [43].

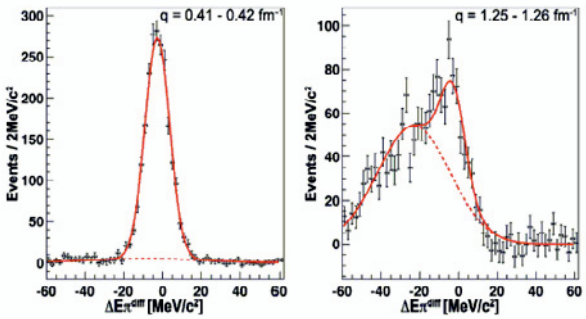


**Figure 11.** Difference between the measured pion energy and the pion energy reconstructed from two-body kinematics. The left-hand panel shows data from the maximum of the diffraction pattern. This data is entirely coherent. The right-hand panel shows data from the diffraction minimum. This data has an appreciable incoherent background which is fitted and subtracted.

Given the variety of results and their dependence on theoretical interpretation, more accurate measurements were needed. Coherent $A(\gamma,\pi^0)A$ reactions offer a new and accurate method to study nuclear matter distributions. Coherent reactions leave the target nucleus in its ground state and the $\pi^0$ are produced coherently on all nucleons, both protons and neutrons. As illustrated in figure 12, the reaction produces a classic diffraction pattern which is sensitive to the nuclear matter radius. In turn this allows the neutron skin thickness to be determined to a high accuracy.

Coherent $\pi^0$ measurements have been made at MAMI on $^{12}C$, $^{16}O$, $^{40}Ca$, $^{208}Pb$ and on three Sn isotopes. Figure 11 shows the difference between the measured pion energy and the energy reconstructed from two-body kinematics for $\pi^0$ production from $^{208}Pb$ at $E_\gamma$=200 MeV. In the diffraction maximum coherent processes dominate, but in the diffraction minimum there are incoherent events present. These are fitted and subtracted.

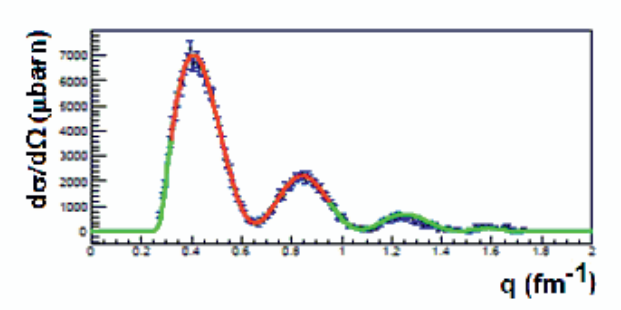


**Figure 12.** Momentum dependence of the $^{208}Pb(\gamma,\pi^0)^{208}Pb$ reaction for photon energies between 190 and 200 MeV. The data are fitted to a model including the pion-nucleus interaction. The red solid line shows the range over which the data are fitted to extract the neutron radius and diffuseness.

Figure 12 shows the momentum dependence of the coherent $^{208}Pb(\gamma,\pi^0)^{208}Pb$ reaction cross section for photon energies between 190 and 200 MeV. The data are fitted to a model including the pion-nucleus interaction [30].

From this model the neutron half-height radius and diffuseness are extracted. The radius is 0.55 ± 0.01(*stat*) ± 0.02(*sys*) fm and the diffuseness is 6.77 ± 0.03(*stat*) ± 0.01(*sys*). From this the neutron skin thickness is calculated to be 0.19 +0.03−0.06(*stat*) +0.04−0.045(*sys*).

The neutron distribution is ~20% more diffuse than the proton distribution in $^{208}Pb$, indicating a tail in the neutron distribution extending to large radii.

## 4 Summary

The world-class facilities at the Mainz 1.6 GeV electron offer access to a wide range of meson photoproduction experiments. In particular its facilities allow measurements of many single- and double-polarisation observables which are essential to a study of pseudoscalar meson photoproduction. This is an essential step in understanding the spectrum of baryon resonances and the structure of excited nucleons.

These same facilities also allow a range of single- and double-polarised Compton scattering experiments, beyond the scope of the present discussion, to be carried out. These are expected to provide information on nucleon vector polarisibilities and will yield valuable new insights into the ground state properties of nucleons, the basic building blocks of matter.

The future programme at Mainz will include extensions of the present double-polarisation meson photoproduction measurements as well as detailed measurements of the complementary Compton scattering reactions.

## Acknowledgements

The author would like to thank many colleagues within the A2-CB collaboration for providing material included in this presentation.

## References

1. K.-H. Kaiser et al., Nucl. Instrum. Methods A **593**, 159 (2008)
2. A. Jankowiak, Eur. Phys. J. A **28**, s1.149 (2006)
3. J.C. McGeorge et al., Eur. Phys. J. A **37**, 129 (2008).
4. I. Anthony et al., Nucl. Instrum. Methods A **301**, 230 (1991)
5. S.J. Hall et al., Nucl. Instrum. Methods A **368**, 698 (1996)
6. M. Unversagt et al., "*Decays of the η' meson," Mainz PAC proposal* A2-02 (2009)
7. A. Reiter et al., Eur. Phys. J. A **30,** 461 (2006)
8. U. Timm, Fortschr. Phys. **17**, 765 (1969)
9. D. Lohmann et al., Nucl. Instrum. Methods A **343**, 494 (1994)
10. K. Livingston, Nucl. Instrum. Methods A **603**, 205 (2009)
11. A. Starostin et al., Phys. Rev. C **64**, 055205 (2001)
12. R. Novotny, IEEE Trans. Nucl. Sci. **38**, 379 (1991)
13. A.R. Gabler et al., Nucl. Instrum. Methods A **346**, 168 (1994)
14. D.P. Watts, *Proc. 11th Intl. Conf. on Calorimetry in High Energy Physics* 116 (2004)
15. S. Janssen et al., IEEE Trans. Nucl. Sci. **47**, 798 (2000)
16. A. Thomas, *Proc. 14th Intl. Workshop on Polarized Sources, Targets and Polarimetry*, ISBN 978-5-86763-282-3, 139 (2011)
17. M. Sikora et al., Phys. Rev. Lett. (accepted for publication)
18. N. Isgur and G. Karl, Phys. Lett. B **72**, 109 (1977); Phys. Rev. D **18**, 4187 (1978); Phys. Rev. D **19**, 2653 (1979), Phys. Rev. D **23**, 817(E) (1981)
19. R. Koniuk and N. Isgur, Phys. Rev. D **21**,1868 (1980)
20. I.S. Barker, A. Donnachie, and J.K. Storrow, Nucl. Phys. B **95**, 347 (1975)
21. W.-T. Chiang and F. Tabakin, Phys. Rev. C **55**, 2054 (1997).
22. V. Kuznetsov V and M. Polyakov JETP Lett. **88**, 347 (2008)
23. I. Jaegle et al., Phys. Rev. Lett. **100**, 252002 (2008)

24. H. Kim, Phys. Rev. D **7,** 094023 (2005)
25. J. Mancell, *A Study of η Photoproduction on the Proton at MAMI, PhD thesis, University of Glasgow* (2012)
26. J. Mancell and I.J.D. MacGregor, *η Photoproduction on the Proton, Proc. Rutherford Cent. Conf. on Nuclear Physics*, J. Phys: Conf. Ser. **381** 012024 (2012)
27. T.C. Jude et al., arXiv:1308.5659 (2013)
28. K.H. Glander et al., Eur. Phys. J. A **19**, 251 (2004)
29. R. Bradford et al., Phys. Rev. C **73** 035202 (2006)
30. B. Dey et al., Phys. Rev. C **82** 025202 (2010)
31. M.E. McCracken et al., Phys. Rev. C **81** 025201 (2010)
32. C. M. Tarbert et al., arXiv:1311.0168 (2013)
33. F. Tondeur et al., Nucl. Phys. A **420**, 297 (1984)
34. J. Zenihiro et al., Phys. Rev. C **82**, 044611 (2010)
35. E. Friedman, Nucl. Phys. A **896** 46 (2012)
36. B. Kos et al., Phys. Rev. C **76**, 014311 (2007)
37. B. A. Brown et al., Phys. Rev. C **76**, 034305 (2007)
38. W. Chen, C. M. Ko and B. A. Li, Phys. Rev. C **72**, 064309 (2005)
39. A. Carbone et al., Phys. Rev. C **81**, 041301(R) (2010)
40. A. Tamii et al., Phys. Rev. Lett. **107**, 062502 (2011)
41. A. Krasznahorkay et al., Phys. Rev. Lett. **66**, 1287 (1991); arXiv:1311.1456 (2013)
42. P. Reinhard and V. Nazarewicz, Phys. Rev. C **81**, 051303(R) (2010)
43. S. Abrahamyan et al., Phys. Rev. Lett. **108**, 112502 (2012)